4. R. D. Richardson, E. J. Holland, B. K. Carpenter, *Nat. Chem.* **3**, 301–303 (2011).
5. B. A. Rosen *et al.*, *Science* **334**, 643–644 (2011).
6. L. Zhang, D. Zhu, G. M. Nathanson, R. J. Hamers, *Angew. Chem. Int. Ed.* **53**, 9746–9750 (2014).
7. D. Gao *et al.*, *J. Am. Chem. Soc.* **137**, 4288–4291 (2015).
8. H. Mistry *et al.*, *J. Am. Chem. Soc.* **136**, 16473–16476 (2014).
9. R. Reske, H. Mistry, F. Behafarid, B. Roldan Cuenya, P. Strasser, *J. Am. Chem. Soc.* **136**, 6978–6986 (2014).
10. W. Zhu *et al.*, *J. Am. Chem. Soc.* **135**, 16833–16836 (2013).
11. A. Salehi-Khojin *et al.*, *J. Phys. Chem. C* **117**, 1627–1632 (2013).
12. M. Asadi *et al.*, *Nat. Commun.* **5**, 4470 (2014).
13. See supplementary materials on *Science* Online.
14. J. L. DiMeglio, J. Rosenthal, *J. Am. Chem. Soc.* **135**, 8798–8801 (2013).
15. B. Kumar *et al.*, *Nat. Commun.* **4**, 2819 (2013).
16. B. A. Rosen, W. Zhu, G. Kaul, A. Salehi-Khojin, R. I. Masel, *J. Electrochem. Soc.* **160**, H138–H141 (2012).
17. Y. Chen, C. W. Li, M. W. Kanan, *J. Am. Chem. Soc.* **134**, 19969–19972 (2012).
18. C. W. Li, M. W. Kanan, *J. Am. Chem. Soc.* **134**, 7231–7234 (2012).
19. D. A. Lutterman, Y. Surendranath, D. G. Nocera, *J. Am. Chem. Soc.* **131**, 3838–3839 (2009).
20. S. Y. Reece *et al.*, *Science* **334**, 645–648 (2011).
21. M. W. Kanan, D. G. Nocera, *Science* **321**, 1072–1075 (2008).
22. Y. Tan *et al.*, *Adv. Mater.* **26**, 8023–8028 (2014).
23. D. J. Li *et al.*, *Nano Lett.* **14**, 1228–1233 (2014).
24. J. Kibsgaard, Z. Chen, B. N. Reinecke, T. F. Jaramillo, *Nat. Mater.* **11**, 963–969 (2012).
25. G. Fishman, D. Calecki, *Phys. Rev. Lett.* **62**, 1302–1305 (1989).
26. T. Fujita *et al.*, *Phys. Rev. Lett.* **101**, 166601 (2008).
27. C. Gong *et al.*, *ACS Nano* **7**, 11350–11357 (2013).
28. J. K. Nørskov *et al.*, *J. Phys. Chem. B* **108**, 17886–17892 (2004).
29. H. A. Hansen, J. B. Varley, A. A. Peterson, J. K. Nørskov, *J. Phys. Chem. Lett.* **4**, 388–392 (2013).
30. A. A. Peterson *et al.*, *Energy Environ. Sci.* **3**, 1311 (2010).
31. B. Hammer, J. K. Nørskov, *Adv. Catal.* **45**, 71–129 (2000).
32. B. Hammer, J. K. Norskov, *Nature* **376**, 238–240 (1995).
33. C. Tsai, F. Abild-Pedersen, J. K. Nørskov, *Nano Lett.* **14**, 1381–1387 (2014).
34. C. Tsai, K. Chan, F. Abild-Pedersen, J. K. Nørskov, *Phys. Chem. Chem. Phys.* **16**, 13156–13164 (2014).

ACKNOWLEDGMENTS

Supported by NSF grant CBET-1512647 (A.S.-K.); the MRSEC Materials Preparation and Measurement Laboratory shared user facility at the University of Chicago (grant NSF-DMR-1420709); the EPIC facility (NUANCE Center–Northwestern University), which has received support from the MRSEC program (grant NSF-DMR-1121262) at the Materials Research Center; the Nanoscale Science and Engineering Center (NSF EEC-0647560) at the International Institute for Nanotechnology; and the State of Illinois through the International Institute for Nanotechnology. The work at Argonne National Laboratory was supported by the U.S. Department of Energy under contract DE-AC0206CH11357 from the Division of Materials Science and Engineering, Basic Energy Science (P.Z., C.L., and L.A.C.). The authors also acknowledge Analytical Chemistry Laboratory of the Earth and Planetary Sciences Department, University of New Mexico. Author contributions: A.S.-K., M.A., and B.K. conceived the idea; A.S.-K., M.A., K.K., and A.V.A. performed the electrochemical experiments; M.A., P.A., and A.B. grew and synthesized the TMDC flakes; M.A., B.K., and P.Y. did the characterizations; C.L., P.Z., and L.C. performed DFT calculations; P.P. and R.K. carried out STEM and electron energy loss spectroscopy; R.H. performed UPS experiments; J.M.C. performed elemental analysis measurement; J.A. and A.S.K. jointly supervised M.A.'s efforts; and all authors contributed to the manuscript before submission. A.S.-K., M.A., and B.K. have filed a provisional patent application. The other authors declare no competing financial interests.

SUPPLEMENTARY MATERIALS

www.sciencemag.org/content/353/6298/467/suppl/DC1
Materials and Methods
Figs. S1 to S27
Tables S1 to S7
References (*35*–*53*)

14 February 2016; accepted 1 July 2016
10.1126/science.aaf4767

PALEOCEANOGRAPHY

North Atlantic ocean circulation and abrupt climate change during the last glaciation

L. G. Henry,[1]* J. F. McManus,[1] W. B. Curry,[2,3] N. L. Roberts,[4] A. M. Piotrowski,[4] L. D. Keigwin[2]

The most recent ice age was characterized by rapid and hemispherically asynchronous climate oscillations, whose origin remains unresolved. Variations in oceanic meridional heat transport may contribute to these repeated climate changes, which were most pronounced during marine isotope stage 3, the glacial interval 25 thousand to 60 thousand years ago. We examined climate and ocean circulation proxies throughout this interval at high resolution in a deep North Atlantic sediment core, combining the kinematic tracer protactinium/thorium (Pa/Th) with the deep water-mass tracer, epibenthic $\delta^{13}C$. These indicators suggest reduced Atlantic overturning circulation during every cool northern stadial, with the greatest reductions during episodic Hudson Strait iceberg discharges, while sharp northern warming followed reinvigorated overturning. These results provide direct evidence for the ocean's persistent, central role in abrupt glacial climate change.

Unlike the relatively stable preindustrial climate of the past 10 thousand years, glacial climate was characterized by repeated millennial oscillations (*1*). These alternating cold stadial and warm interstadial events were most abrupt and pronounced on Greenland and across much of the northern hemisphere, with the most extreme regional conditions during several Heinrich (H) events (*2*), catastrophic iceberg discharges into the subpolar North Atlantic Ocean. These abrupt events not only had an impact on global climate but also are associated with widespread reorganizations of the planet's ecosystems (*3*). Geochemical fingerprinting of the ice-rafted detritus (IRD) associated with the most pronounced of these events consistently indicates a source in the Hudson Strait (HS) (*4*), so we abbreviate this subset of H events as HS events and their following cool periods as HS stadials. During northern stadials, ice cores show that Antarctica warmed, and each subsequent rapid northern hemisphere warming was followed shortly by cooling at high southern latitudes (*5*). Explanations for the rapidity and asynchrony of these climate changes require a mechanism for partitioning heat on a planetary scale, initiated either through reorganization of atmospheric structure (*6*) or the ocean's thermohaline circulation, particularly the Atlantic meridional overturning circulation (AMOC) (*7*–*10*). Coupled climate models have successfully used each of these mechanisms to generate time series that replicate climate variability observed in paleoclimate archives (*9*, *11*). We investigated the relationship between Northern Hemispheric climate as recorded in Greenland ice cores and marine sediments, along with isotopic deep-sea paleoproxies sensitive to changes in North Atlantic Deep Water (NADW) production and AMOC transport during marine isotope stage three (MIS3). Throughout that time, when global climate was neither as warm as today nor as cold as the last glacial maximum (LGM), ice sheets of intermediate size blanketed much of the northern hemisphere, and large millennial stadial-interstadial climate swings (*6*, *8*) provide a wide dynamic range that allows examination of the ocean's role in abrupt change.

Sediment samples were taken from the long (35 m) core KNR191-CDH19—recovered from the Bermuda Rise (33° 41.443' N; 57° 34.559' W, 4541 m water depth) in the northwestern Atlantic Ocean (Fig. 1), near previous seafloor sampling at Integrated Ocean Drilling Program (IODP) site 1063—and coring sites KNR31 GPC-5, EN120 GGC-1, MD95-2036, OCE326-GGC5, and others. Because this region of the deep North Atlantic is characterized by steep lateral gradients in tracers of NADW and Antarctic Bottom Water (AABW), the Bermuda Rise has been intensively used to explore the connection between changes in ocean circulation and climate (*7*, *12*). In this study, we measured the radioisotopes ^{231}Pa and ^{230}Th in bulk sediment, age-corrected to the time of deposition, along with stable carbon ($\delta^{13}C$) and oxygen ($\delta^{18}O$) isotope ratios in the microfossil shells of both epibenthic foraminifera (*Cibicidoides wuellerstorfi* and *Nuttallides umbonifera*) and planktonic foraminifera (*Globigerinoides ruber*), respectively, yielding inferences on relative residence times and the origin of deep water masses on centennial time scales.

Isotopes of protactinium and thorium, ^{231}Pa and ^{230}Th, are produced from the decay of ^{235}U and ^{234}U, respectively, dissolved in seawater. This activity of ^{231}Pa and ^{230}Th in excess of the amount

[1]Lamont-Doherty Earth Observatory (LDEO), Columbia University, Palisades, NY 10964, USA. [2]Woods Hole Oceanographic Institution, Woods Hole, MA 02543, USA. [3]Bermuda Institute of Ocean Sciences, St. George's, Bermuda. [4]University of Cambridge, Department of Earth Sciences, Cambridge CB2 3EQ, UK.
*Corresponding author. Email: lhenry@ldeo.columbia.edu

supported by the decay of uranium within the crystal lattice of the sediment's mineral grains is denoted by $^{231}Pa_{xs}$ and $^{230}Th_{xs}$. Because the parent U isotopes have long residence times, U is well mixed throughout the ocean. This yields a $^{231}Pa_{xs}/^{230}Th_{xs}$ (hereafter Pa/Th) production ratio (Pa/Th = 0.093) that is constant and uniformly distributed (*13*, *14*). Both daughter isotopes are removed by adsorption onto settling particles, with Th more efficiently scavenged than Pa. The residence time of $^{231}Pa_{xs}$ (τ_{res} = ~200 years) in seawater is thus greater than that of $^{230}Th_{xs}$ (τ_{res} = ~30 years), allowing $^{231}Pa_{xs}$ to be redistributed laterally by changes in basin-scale circulation before deposition (*7*, *14*–*16*), with the additional potential influence of removal because of changes in particle rain associated with biological productivity (*17*). Settling particles (*18*) and surface sediments throughout the basin reveal a deficit in $^{231}Pa_{xs}$ burial that is consistent with large-scale export by the deep circulation (Fig. 1) (*19*).

The downcore Pa/Th in core CDH-19 ranges from ~0.05 to slightly above the production ratio of 0.093, with a series of well-defined variations throughout MIS3 (Fig. 2). In sediments deposited during Greenland interstadial intervals (*1*), Pa/Th ratios average 0.0609 ± 0.0074 (2σ), which is substantially below the production ratio (Fig. 2) and only 10% higher than the mean value (Pa/Th = 0.055) of the Holocene, a time of relatively vigorous AMOC (*7*). Because $^{230}Th_{xs}$ is buried in near balance with its production (*20*), the relatively low Pa/Th indicates a substantial lateral export of $^{231}Pa_{xs}$, which is consistent with relatively vigorous AMOC during interstadials, although the vertical integration through the water column of this deficit does not distinguish whether this export occurred at deep or intermediate levels. Epibenthic $\delta^{13}C$ ($\delta^{13}C_{BF}$) data allow discrimination between these two possibilities and display increased values during each interstadial, implying a greater contribution of the isotopically more positive North Atlantic end member (Fig. 2). During these intervals, this positive isotopic signal suggests that a deeper overturning cell was established, rather than a shallower, yet more vigorous one. This confirms a previous suggestion of intervals of relatively strong AMOC within the most recent ice age (*21*, *22*), although Pa/Th and $\delta^{13}C_{BF}$ adjusted for whole-ocean inventory changes (*23*) rarely reach early Holocene values.

Pa/Th increases within each Greenland stadial interval, for a mean duration of 0.531 ± 0.303 thousand years to a Pa/Th value of 0.0797 ± 0.0154, which indicates decreased lateral export of $^{231}Pa_{xs}$ and is consistent with a shallower or reduced overturning cell in the North Atlantic. During these

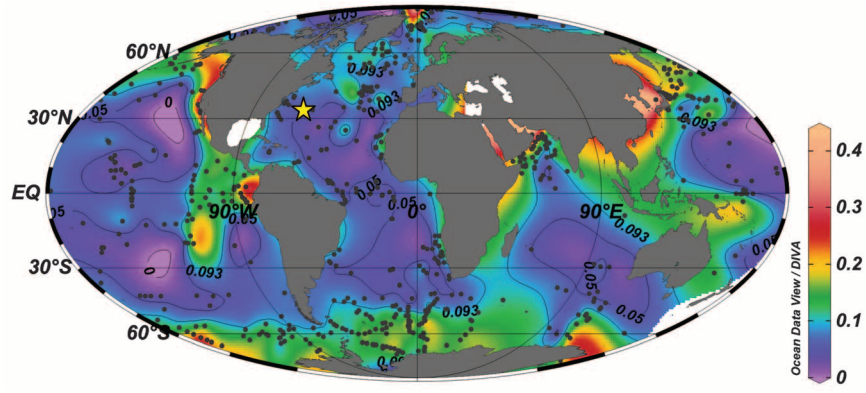

Fig. 1. Study core location and coretop distribution of Pa/Th. Location sediment core CDH19 indicated with a star (33° 41.443' N; 57° 34.559' W, 4541-m water depth), with Pa/Th ratios (black dots) in core top sediments used with Ocean Data View Data-Interpolating Variational Analysis gridding to produce the color contours. White areas contain no data.

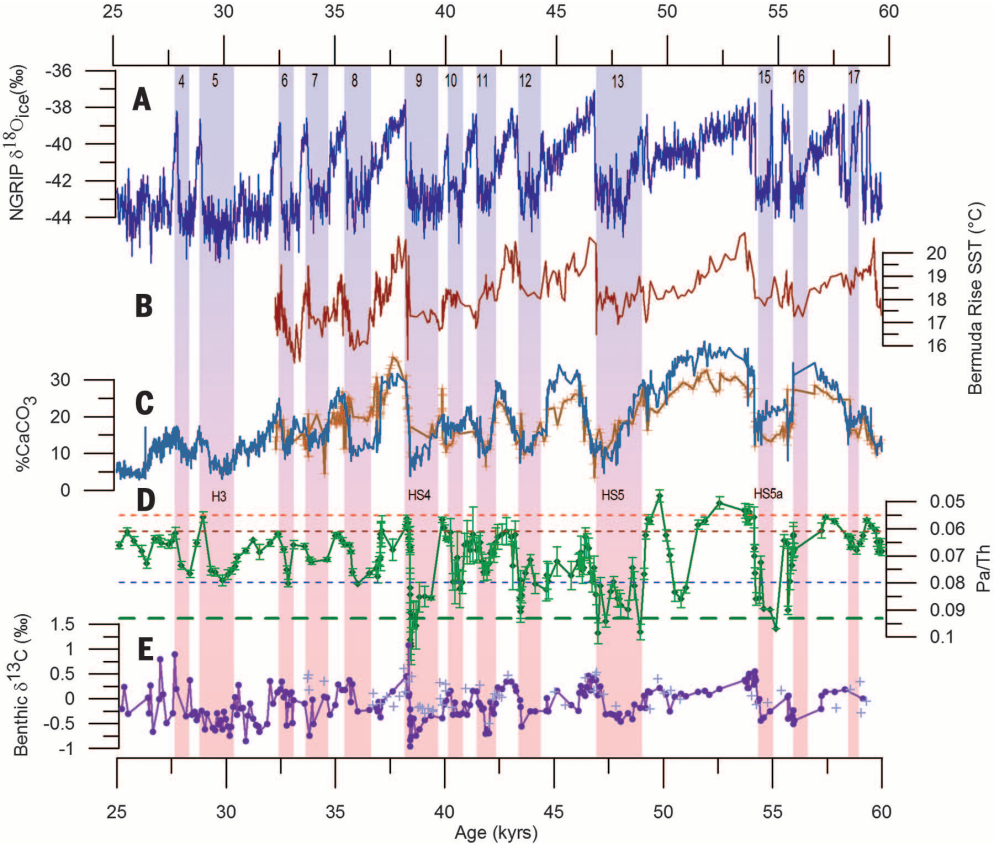

Fig. 2. Climate and circulation indices through MIS3. Stadials are numbered with vertical bars. (**A**) NGRIP ice core $\delta^{18}O_{ice}$ 75.1°N, 42.32°W (*35*). (**B**) SST (°C) from MD95-2036, 33° 41.444'N, 57° 34.548'W, 4462 m (*31*). (**C**) Calcium x-ray fluorescence (orange) from core CDH19 (this study) mapped to $\%CaCO_3$, with calibration r^2 = 0.87 (S.1), with spectral reflectance (blue) from core MD95-2036 (*36*). (**D**) Pa/Th from bulk sediment (green) taken from core CDH19. (**E**) $\delta^{13}C_{BF}$ from core CDH19 (purple) alternates between values consistent with southern and northern sourced $\delta^{13}C_{BF}$ end members.

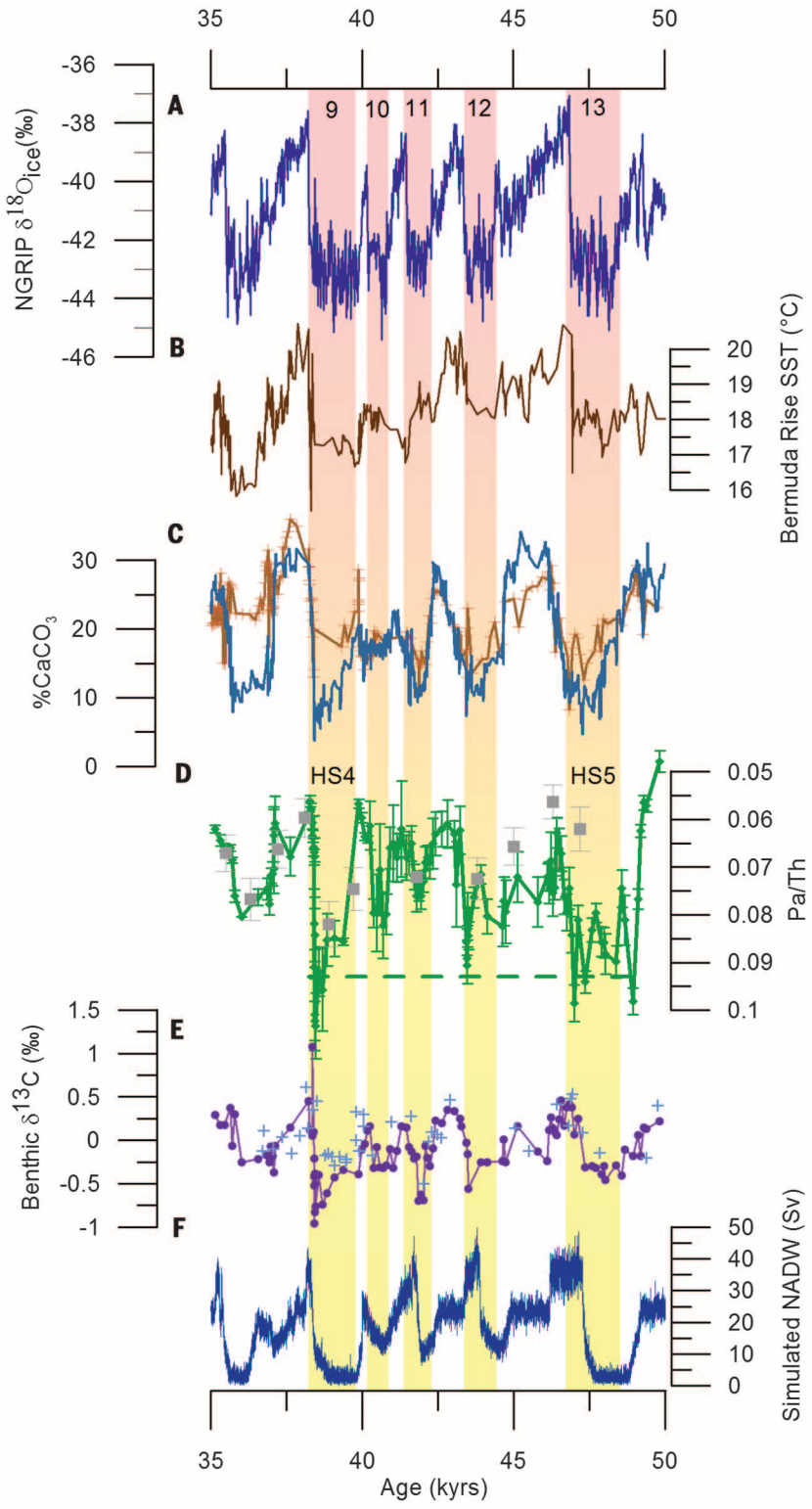

Fig. 3. Detail of millennial cyclicity in glacial climate and the deep ocean. (**A**) through (**E**) are as in Fig. 2, A to E. (**F**) Simulated NADW (Sv) in a coupled ocean/atmosphere model (*11*), with (D) published Pa/Th (gray squares) (*21*) and $\delta^{13}C_{BF}$ data (blue crosses) (*12*).

stadials, $\delta^{13}C_{BF}$ decreases substantially to negative values [−0.2 per mill (‰) to −0.5‰], suggesting greater influence of the glacial equivalent of modern Antarctic Bottom Water (AABW), an isotopic result that is consistent with reduced AMOC from a coupled climate model (*10*). Although the northern and southern water mass end members are not well known throughout the last glaciation, deep waters in the Atlantic during the LGM ranged from less than −0.5‰ in the south to greater than 1.5‰ in the north (*23*). If these values prevailed throughout MIS3, then the low $\delta^{13}C_{BF}$ indicates a dominant stadial influence of southern waters and substantial northward retreat or shoaling of the AABW/NADW mixing zone, which is consistent with the deep water mass configuration that has previously been reconstructed for the LGM (*23*, *24*), although not for millennial-scale stadial intervals within the glaciation.

The mean Pa/Th of both stadials and interstadials is consistent with export of $^{231}Pa_{xs}$ from the subtropical North Atlantic during most of MIS3. During peak interstadials, when low Pa/Th indicates the local burial of approximately half of $^{231}Pa_{xs}$ production, the remaining half would have been exported. In contrast, the substantial decrease in the lateral export of $^{231}Pa_{xs}$ evident in higher Pa/Th, along with lower $\delta^{13}C_{BF}$ during each stadial interval, points to repeated reductions in AMOC and its attendant northward heat transport throughout MIS3. The contrast between apparent deep, vigorous overturning during interstadials and shallower (*25*), weaker overturning during stadials is most pronounced in conjunction with all HS stadials (Fig. 2), when catastrophic discharge of melting icebergs from Canada flooded the subpolar North Atlantic (*4*).

Sediments deposited during HS stadials are characterized by a mean duration of 1.65 ± 0.545 thousand years and an average Pa/Th of 0.095 ± 0.016, which is indistinguishable from the production ratio. These results therefore indicate no net export of $^{231}Pa_{xs}$ from the subtropical North Atlantic during these events sourced from the Hudson Strait. This balance between seawater radiometric production and underlying sedimentary burial would be expected under conditions with a substantial reduction in AMOC or other lateral transport and might imply a near cessation of $^{231}Pa_{xs}$ export through deep circulation. Although variable scavenging may also contribute to sedimentary Pa/Th, values throughout MIS3 bear only a weak relationship with bulk and opal fluxes [coefficient of determination (r^2) = 0.19] (*19*), which therefore constitute secondary influences.

These new results reveal that AMOC variations were associated with every MIS3 stadial-interstadial oscillation, with the largest reductions during HS stadials. The well-resolved interval 35 thousand to 50 thousand years ago provides a good example (Fig. 3). This iconic interval contains H4, H5, and the intervening series of oscillations that have served as a basis for conceptual and computer models seeking to explain such variability (*8*–*11*, *26*, *27*). A previous Pa/Th record (*21*) covering this interval captured much of the overall amplitude, and the new data resolve each stadial increase in Pa/Th, indicating that only HS4 and HS5 reach the production ratio of 0.093. Because the interstadial values are similar to each other, the subsequent abrupt increases in AMOC and regional warming are also the greatest and occur

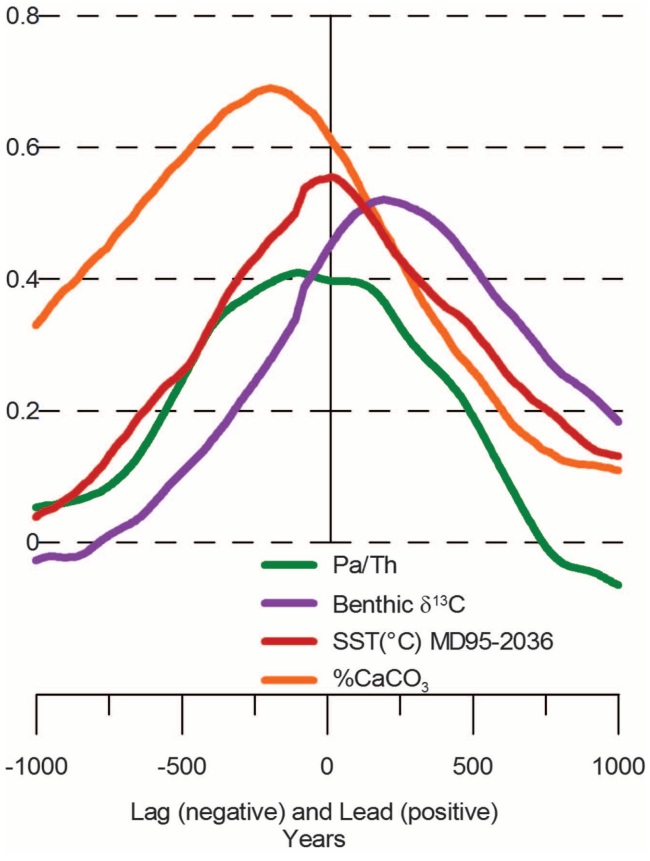

Fig. 4 Phasing lag correlations. Correlation of NGRIP ice core $\delta^{18}O$ with CDH19 $\%CaCO_3$ (orange), Pa/Th of bulk sediment from CDH19 (green), $\delta^{13}C_{BF}$ from CDH19 (purple), and SST °C from MD95-2036 (*31*) (red).

within the century-scale response time of Pa/Th. Throughout the records, the Pa/Th and $\delta^{13}C_{BF}$ bear a striking similarity to model output forced by freshwater anomalies (*11*).

Combined with previous investigations (*7*, *28*), these new results confirm that all HS events of the past 60 thousand years were associated with a dramatic increase in Pa/Th and are evidence for major reduction in AMOC in association with the largest IRD events (*29*). In contrast, H3, the sole Heinrich event stadial that fails to reach the production ratio (peak Pa/Th = 0.079), displays smaller IRD fluxes across the subpolar Atlantic (*29*), with provenance inconsistent with a Hudson Strait source (*4*). This muted result for H3 is consistent with evidence from the Florida Straits (*30*) showing a smaller reduction at that time in the northward flow of near-surface waters that feed the overturning circulation. As with all stadials, the HS events are characterized by lower $\delta^{13}C_{BF}$, suggesting diminished influence of NADW and proportionately greater AABW on Bermuda Rise. Combined Pa/Th and $\delta^{13}C_{BF}$ results therefore indicate a persistent pattern of stadial weakening and interstadial strengthening, with a repeatedly largest reduction in AMOC associated with all HS events. Although these observations are consistent with a number of numerical model simulations (*11*, *27*) as well as conceptual models for the mechanisms of abrupt change, they have previously been difficult to document and fully resolve.

Recent data from the Western Antarctic ice sheet provide compelling evidence for a robust lead of Greenland climate over Antarctica (*5*). That analysis revealed a Northern Hemisphere lead of 208 ± 96 years, indicating that the interhemispheric teleconnection propagates from north to south on time scales consistent with basin-scale ocean circulation. To ascertain whether Northern Hemisphere climate is forced or reinforced by changes in AMOC, we investigated the phase relationship between surface and deep-sea properties. Cross-correlations were performed on each of $\delta^{13}C_{BF}$, Pa/Th, sea surface temperature (SST), and $CaCO_3$ with North Greenland Ice Core Project (NGRIP) $\delta^{18}O$ from both sediment cores CDH19 and MD95-2036 from the Bermuda Rise. The optimal correlation of $\delta^{13}C_{BF}$ leads NGRIP $\delta^{18}O$ by approximately 2 centuries (Fig. 4). This lead is corroborated by Pa/Th phasing, which when considering the century-scale response time of the proxy (*13*, *14*) is consistent with AMOC changes indicated by $\delta^{13}C_{BF}$. The SST reconstruction from MD95-2036 was aligned with Greenland $\delta^{18}O$, yielding a correlation of $r^2 = 0.83$ (*31*). SST and Pa/Th are synchronous with NGRIP to within the estimated bioturbation error of 8 cm within the core, displaying correlations with Greenland of $r^2 = 0.47$ for Pa/Th and $r^2 = 0.65$ for SST. The optimal correlation of $\%CaCO_3$, $r^2 = 0.64$, lags NGRIP $\delta^{18}O$ by nearly 200 years.

The consistent lead of variations in $\delta^{13}C_{BF}$ before SST and Greenland temperatures, repeated over multiple millennial cycles, indicates the potential influence of AMOC on NH climate and confirms that the Bermuda Rise is exposed to shifts in deep-water mass mixing. Initially, deep circulation changes, which is evidenced overall by the timing of $\delta^{13}C_{BF}$. Pa/Th shifts are essentially in tandem with regional temperature when circulation accelerates, and soon thereafter as it responds to weakening AMOC (*19*). Given the response time of Pa/Th to instantaneous shifts in North Atlantic overturning (*13*, *14*), this also suggests that changes in AMOC precede regional temperature change, although the exact timing may have differed during cooling and warming phases. Both SST and Greenland temperature proxies lag the ocean circulation in a consistent fashion, and in turn, these northern changes have been demonstrated to lead Antarctic temperatures (*5*). Calcium-carbonate concentration is the last of the proxies to respond to AMOC change, which is consistent with the longer time scale of preservation, dissolution, and dilution in the deep ocean.

The relative timing of the observed AMOC changes has important implications for regional and global climate. Whereas numerous computer simulations suggest that melting icebergs and other freshwater input associated with H events may have shut down NADW production (*9*, *11*, *27*), recent results examining the phasing of North Atlantic SST and IRD suggest that stadial conditions began to develop before ice-rafting (*32*). The evidence here nevertheless indicates that the greatest AMOC reduction and the coldest stadial intervals accompanied the largest iceberg discharges. This suggests that the iceberg discharges may have provided a positive feedback mechanism to accelerate the initial cooling within each multimillennial climate cycle. In addition, the extended H-stadial reductions in AMOC observed in this study coincide with intervals of rising atmospheric CO_2 (*33*), whereas CO_2 declined when AMOC increased during the subsequent sharp transitions to northern interstadials, supporting a potential influence on the atmosphere by the deep circulation on millennial time scales (*34*).

The robust relationship of reductions in export of northern deep waters evident in reduced $^{231}Pa_{xs}$ export and decreased $\delta^{13}C_{BF}$ before and during stadial periods, and the dramatic increases in both during interstadials, provide direct evidence for the role of AMOC in abrupt glacial climate change. The sequence of marked circulation changes and northern hemisphere climate detailed here, combined with the demonstrated lag of Antarctic temperature variations (*5*), strongly implicates changes in meridional heat transport by the ocean as a trigger for abrupt northern hemisphere warming and the tipping of the "bipolar seesaw" (*26*).

REFERENCES AND NOTES

1. W. Dansgaard *et al.*, *Nature* **364**, 218–220 (1993).
2. W. Broecker, G. Bond, M. Klas, E. Clark, J. McManus, *Clim. Dyn.* **6**, 265–273 (1992).
3. M. Yasuhara, T. M. Cronin, P. B. Demenocal, H. Okahashi, B. K. Linsley, *Proc. Natl. Acad. Sci. U.S.A.* **105**, 1556–1560 (2008).
4. S. R. Hemming, *Rev. Geophys.* **42**, RG1005 (2004).
5. C. Buizert *et al.*, *Nature* **520**, 661–665 (2015).
6. X. Zhang, G. Lohmann, G. Knorr, C. Purcell, *Nature* **512**, 290–294 (2014).
7. J. F. McManus, R. Francois, J. M. Gherardi, L. D. Keigwin, S. Brown-Leger, *Nature* **428**, 834–837 (2004).
8. R. B. Alley, P. Clark, L. Keigwin, R. Webb, *Geophys. Monog. Ser.* **112**, 385–394 (1999).
9. S. Rahmstorf, *Nature* **419**, 207–214 (2002).
10. A. Schmittner, D. C. Lund, *Clim. Past* **11**, 135–152 (2015).
11. L. Menviel, A. Timmermann, T. Friedrich, M. H. England, *Clim. Past* **10**, 63–77 (2014).
12. L. Keigwin, E. Boyle, *Paleoceanography* **14**, 164–170 (1999).
13. G. M. Henderson, R. F. Anderson, *Rev. Mineral. Geochem.* **52**, 493–531 (2003).
14. E. F. Yu, R. Francois, M. P. Bacon, *Nature* **379**, 689–694 (1996).
15. C. Negre *et al.*, *Nature* **468**, 84–88 (2010).

16. J. M. Gherardi *et al.*, *Paleoceanography* **24**, PA2204 (2009).
17. R. F. Anderson *et al.*, *Science* **323**, 1443–1448 (2009).
18. C. Hayes *et al.*, *Mar. Chem.* **170**, 49–60 (2015).
19. Materials and methods are available as supplementary materials on *Science* Online.
20. G. M. Henderson, C. Heinze, R. F. Anderson, A. M. E. Winguth, *Deep Sea Res. Part I Oceanogr. Res. Pap.* **46**, 1861–1893 (1999).
21. E. Böhm *et al.*, *Nature* **517**, 73–76 (2015).
22. J. Gottschalk *et al.*, *Nat. Geosci.* **8**, 950–954 (2015).
23. W. B. Curry, D. W. Oppo, *Paleoceanography* **20**, PA1017 (2005).
24. J. F. Adkins, *Paleoceanography* **28**, 539–561 (2013).
25. R. Zahn, A. Stüber, *Earth Planet. Sci. Lett.* **200**, 191–205 (2002).
26. W. Broecker, *Paleoceanography* **13**, 119–121 (1998).
27. A. Ganopolski, S. Rahmstorf, *Nature* **409**, 153–158 (2001).
28. J. Lippold *et al.*, *Geophys. Res. Lett.* **36**, L12601 (2009).
29. J. F. McManus, R. F. Anderson, W. S. Broecker, M. Q. Fleisher, S. M. Higgins, *Earth Planet. Sci. Lett.* **155**, 29–43 (1998).
30. J. Lynch-Stieglitz *et al.*, *Nat. Geosci.* **7**, 144–150 (2014).
31. J. P. Sachs, S. J. Lehman, *Science* **286**, 756–759 (1999).
32. S. Barker *et al.*, *Nature* **520**, 333–336 (2015).
33. J. Ahn, E. J. Brook, *Science* **322**, 83–85 (2008).
34. A. Schmittner, E. D. Galbraith, *Nature* **456**, 373–376 (2008).
35. A. Svensson *et al.*, *Clim. Past* **4**, 47–57 (2008).
36. E. A. Boyle, *Proc. Natl. Acad. Sci. U.S.A.* **94**, 8300–8307 (1997).

ACKNOWLEDGMENTS

Data are available at www.ncdc.noaa.gov/paleo/study/20248. This research was supported in part by a NSF Graduate Research Fellowship to L.G.H., by awards from the Comer Science and Education Foundation and NSF grant ATM-0936496 to J.F.M., and an award from the LDEO Climate Center to L.G.H. and J.F.M. L.D.K. and W.B.C. were supported by NSF grant ATM-0836472, and L.D.K. was supported by NSF grant AGS-1548160. We thank M. Jeglinski and K. Rose for technical support. The authors thank R. Anderson, S. Hemming, and C. Hayes for constructive discussion leading to improvement of the manuscript; R. Anderson for unpublished data included in the Fig. 1 map; and M. Fleisher for analytical support.

SUPPLEMENTARY MATERIALS

www.sciencemag.org/content/353/6298/470/suppl/DC1
Materials and Methods
SupplementaryText
Figs. S1 to S7
References (*37*–*55*)
Database S1

29 February 2016; accepted 20 June 2016
10.1126/science.aaf5529

EDUCATION

Teaching accreditation exams reveal grading biases favor women in male-dominated disciplines in France

Thomas Breda[1,2]*† and Mélina Hillion[1,3]†

Discrimination against women is seen as one of the possible causes behind their underrepresentation in certain STEM (science, technology, engineering, and mathematics) subjects. We show that this is not the case for the competitive exams used to recruit almost all French secondary and postsecondary teachers and professors. Comparisons of oral non–gender-blind tests with written gender-blind tests for about 100,000 individuals observed in 11 different fields over the period 2006–2013 reveal a bias in favor of women that is strongly increasing with the extent of a field's male-domination. This bias turns from 3 to 5 percentile ranks for men in literature and foreign languages to about 10 percentile ranks for women in math, physics, or philosophy. These findings have implications for the debate over what interventions are appropriate to increase the representation of women in fields in which they are currently underrepresented.

Why are women underrepresented in most areas of science, technology, engineering, and mathematics (STEM)? One of the most common explanations is that a hiring bias against women exists in those fields (*1*–*4*). This explanation is supported by a few older experiments (*5*–*7*), a recent one with fictitious resumes (*8*), and a recent lab experiment (*9*), which suggest that the phenomenon still prevails.

However, some scholars have challenged this view (*10*, *11*), and another recent experiment with fictitious resumes finds a bias in favor of women in academic recruitment (*12*). Studies based on actual hiring also find that when women apply to tenure-track STEM positions, they are more likely to be hired (*13*–*18*). However, those studies do not control for applicants' quality and a frequent claim is that their results simply reflect that only the best female Ph.D.'s apply to these positions, whereas a larger fraction of males do so (*11*, *13*). A study by one of us did partly control for applicants' quality and reported a bias in favor of women in male-dominated fields (*19*). However, it has limited external validity because it relies on only 3000 candidates who took the French Ecole Normale Supérieure entrance exam.

The present analysis is based on a natural experiment involving >100,000 individuals who participated in competitive exams used to hire French primary, secondary, and college or university teachers over the period 2006–2013. It has two distinct advantages over all previous studies. First, it provides large-scale real-world evidence of gender biases in evaluation-based hiring in several fields. Second, it shows that those biases against or in favor of women are strongly shaped by the actual degree of female underrepresentation in the field in which the evaluation takes place, which partly reconciles existing studies.

Carefully taking into account the extent of underrepresentation of women in 11 academic fields allowed us to extend the analysis beyond the STEM distinction. As pointed out recently (*11*, *12*, *19*, *20*), the focus on STEM versus non-STEM fields can be misleading for understanding female underrepresentation in academia, as some STEM fields are not dominated by men [e.g., 54% of U.S. Ph.D.'s in molecular biology are women (*21*)], whereas some non-STEM fields, including humanities, are male-dominated [e.g., only 31% of U.S. Ph.D.'s in philosophy are women (*21*)]. A better predictor of this underrepresentation, some have argued, is the belief that innate raw talent is the main requirement to succeed in the field (*20*).

To study how female underrepresentation can shape skills assessment, we exploit the two-stage design of the three national exams used in France to recruit virtually all primary-school teachers, CRPE middle- and high-school teachers, CAPES and Agrégation; as well as a large share of graduate school and university teachers, who also take the Agrégation (*22*). A college degree is necessary to take part in those competitive exams [table S1 in (*22*)]. Except for the lower level (CRPE), each exam is subject-specific and typically includes two or three written tests. The best candidates after those written tests (tables S2 and S3) are eligible for typically two or three oral tests taken no later than 3 months after the written tests (*22*). Note that oral tests are not general recruiting interviews: Depending on the subject, they include exercises, questions, or text discussions designed to assess candidates' fundamental skills, exactly as written tests. Teachers or professors who have specialized in the subject grade all the tests. At the highest-level exam (Agrégation), 80% of evaluators are either full-time researchers or university professors in French academia. The corresponding statistic is 30% for the medium-level exam (CAPES).

Our strategy exploits the "blinding" of the written tests (candidates' name and gender are not known by the professors who grade these tests), whereas the oral tests are not blinded. If one assumes that female handwriting cannot be easily detected—which we discuss later—written tests

[1]Paris School of Economics, 48 Boulevard Jourdan, Paris 75014, France. [2]CNRS, UMR8545, Paris-Jourdan Sciences-Economiques, 48 Boulevard Jourdan, Paris 75014, France. [3]Center for Research in Economics and Statistics (CREST), 15 Boulevard Gabriel Péri, Malakoff 92245, France.
*The authors contributed equally to this work. †**Corresponding author. Email: thomas.breda@ens.fr (T.B.); melina.hillion@gmail.com (M.H.)**

North Atlantic ocean circulation and abrupt climate change during the last glaciation

L. G. Henry, J. F. McManus, W. B. Curry, N. L. Roberts, A. M. Piotrowski and L. D. Keigwin

Science **353** (6298), 470-474.
DOI: 10.1126/science.aaf5529originally published online June 30, 2016

An ocean of climate impacts

Large decreases in Atlantic meridional overturning circulation accompanied every one of the cold Northern Hemispheric stadial events that occurred during the heart of the last glacial period. These events, lasting on average around 1000 years each, have long been thought to result from changes in deep ocean circulation. Henry *et al.* used a suite of geochemical proxies from marine sediments to show that reductions in the export of northern deep waters occurred before and during stadial periods (see the Perspective by Schmittner). This observation firmly establishes the role of ocean circulation as a cause of abrupt glacial climate change during that interval.

Science, this issue p. 470; see also p. 445